Lgl resets Par complex membrane loading at mitotic exit to polarize neural stem cells

Bryce LaFoya*, Sarah E. Welch*, and Kenneth E. Prehoda[1]

Institute of Molecular Biology
Department of Chemistry and Biochemistry
1229 University of Oregon
Eugene, OR 97403

*contributed equally

[1]Corresponding author: prehoda@uoregon.edu

Summary

The Par complex regulates cell polarity in diverse animal cells, but how its localization is restricted to a specific membrane domain remains unclear. We investigate how the tumor suppressor Lethal giant larvae (Lgl) regulates Par complex polarity in *Drosophila* neural stem cells (NSCs). Unlike in epithelial cells, where Lgl and the Par complex show mutual exclusion, in NSCs the Par complex is apically polarized while Lgl is cytoplasmic during mitosis. We demonstrate that Lgl's primary function is to remove the Par complex from the membrane at mitotic exit, resetting polarity for the next cell cycle. In Lgl-depleted NSCs, the Par complex persists on both apical and basal membranes throughout the cell cycle. Surprisingly, apical Par complex targeting and polarization occur independently of Lgl, but residual basal Par complex is sufficient to disrupt asymmetric division. These findings reveal a novel mechanism of negative polarity regulation by Lgl and highlight the importance of the pre-polarized state in Par-mediated polarity.

Introduction

Cortical polarity is a fundamental cellular characteristic that underlies diverse biological processes, including directional cell migration, tissue organization, and asymmetric cell division. The Par complex, consisting of Par-6 and atypical Protein Kinase C (aPKC), plays a pivotal role in establishing and maintaining polarity in a wide range of animal cells, from epithelial cells to neurons[1–4]. The proper localization and function of the Par complex are particularly critical in stem cells, where asymmetric distribution of cell fate determinants governs the delicate balance between self-renewal and differentiation. A fundamental question in cell polarity research is how the Par complex itself is restricted to specific membrane domains. The tumor suppressor Lethal giant larvae (Lgl) plays a key role in Par polarity by restricting the Par complex to the proper membrane domain[5–8], but how Lgl controls Par complex localization remains an open question.

Par polarity results from the complex interplay of positive and negative regulators. While positive regulators like Par-3 (Bazooka in *Drosophila*) and Cdc42 ensure that the Par complex is targeted to the membrane[9–11], the negative regulation provided by Lgl is thought to arise from mutual exclusion, where the Par complex and Lgl reciprocally control each other's localization[4]. This model is exemplified by interphase epithelial cells, where the Par complex is confined to the apical plasma membrane while Lgl occupies the basolateral domain (Fig. 1A). The importance of this mutual regulation is evident when Lgl function is lost: in Lgl mutants the Par complex loses its domain specificity and spreads into the

basolateral domain[5,6,8]. Conversely, in Par complex mutants, Lgl is no longer restricted to the basolateral membrane and becomes uniformly distributed across the entire cell surface, including the apical domain. The Par complex regulates Lgl localization through phosphorylation by aPKC[12,13]. Phosphorylation reduces Lgl's affinity for the membrane, ensuring that it only binds membrane regions that lack Par activity. While the Par complex controls Lgl localization by coupling phosphorylation to a decrease in membrane affinity, little is known about how Lgl regulates Par complex localization.

Like epithelial cells, sensory organ precursor (SOP) cells and neural stem cells (NSCs) require Lgl function for proper Par complex polarity[14,15]. However, the dynamics of Par complex localization in these cell types differ significantly from those in epithelial cells (Fig. 1A). In contrast to epithelial cells, where the Par complex is polarized throughout the cell cycle, the Par complex in SOPs and NSCs is not polarized during interphase but becomes polarized during mitosis[5,15]. For example, in NSCs the Par complex localizes to the apical membrane at metaphase where it directs fate determinants like Prospero to the basal side, ultimately leading to asymmetric sibling cell fates[16,17]. In Lgl mutant SOPs and NSCs, the Par complex is localized across the entire membrane instead of being restricted to its proper domain[14], suggesting that Lgl is required for the asymmetric targeting of the Par complex. Importantly, SOPs and NSCs do not conform to the mutual exclusion model observed in epithelial cells. While Lgl is removed from the membrane early in mitosis in all these cell types, the critical difference lies in the timing of Par complex polarization. By metaphase, when the Par complex becomes polarized in SOPs and NSCs, Lgl is no longer present on the membrane[5,15]. This temporal separation between Lgl membrane dissociation and Par complex polarization challenges the idea of direct mutual exclusion between these proteins in SOPs and NSCs, raising questions about how Lgl regulates Par complex localization in these cell types.

Given that disruptions in cell polarity are frequently associated with tumorigenesis, and that Lgl is a known tumor suppressor, unraveling its mode of action and localization patterns may offer new perspectives on the links between polarity, asymmetric division, and cancer development. We examined Lgl and Par complex dynamics in NSCs to resolve the discrepancy between the mutual exclusion model and Lgl's function in these cells. Our findings shed light on the molecular basis of Lgl's function as a negative regulator of Par polarity and provide insights into the broader principles governing cell polarization in diverse cellular contexts.

Results

Patterned Lgl membrane displacement in early NSC mitosis

Lethal giant larvae (Lgl) is bound to the plasma membrane during interphase and becomes cytoplasmic during mitosis in neural stem cells (NSCs)[5]. We sought to determine the dynamics of Lgl's transition between these states including how it is restored to the membrane following mitosis. We examined Lgl's localization throughout the cell cycle NSCs from *Drosophila* larval brain explants using rapid, super-resolution spinning disk confocal microscopy (Fig. 1B). We imaged NSCs expressing Lgl-GFP (expressed by Worniu-GAL4 driven UAS) and RFP-Histone H2A (expressed from its endogenous locus) to visualize Lgl localization relative to cell cycle progression. Lgl removal from the membrane began in early prophase, initiating at a small area near the apical pole of the cell (Fig. 1C,D; Video 1). The removal from the membrane spread rapidly across the cell surface and the apically-initiated pattern gave rise to a state in which Lgl is polarized to the basal membrane. However, this state is short-lived as Lgl removal continued without any apparent delay such that it appeared to be completely displaced into the cytoplasm by late prophase and could be observed both in medial sections and maximum intensity projections of the full cell volume (Fig. 1E). The full volume data also revealed how Lgl displacement from the membrane was affected by the membrane structures that are present on the NSC surface[18–20]. These structures were enriched with Lgl, consistent with their higher density of membrane, and Lgl displacement from the structures proceeded with the same overall dynamics as the surrounding membrane (Fig. 1E). To confirm that Lgl was completely removed from the basal membrane, we imaged individual cultured NSCs that had been dissociated from brains. The Lgl dynamics in dissociated NSCs were consistent with our initial observations of apically-directed membrane clearing and provided unambiguous evidence that Lgl is indeed completely removed from the membrane by late prophase (Fig. 1F,G). The patterned Lgl membrane displacement dynamics indicate that removal is a spatially regulated process, like that observed for SOPs[15], rather than one in which it is simultaneously removed from across the entire cell surface.

NSCs undergo repeated cycles of asymmetric division such that Lgl must be restored to the membrane at some point to achieve its interphase localization state. We analyzed Lgl dynamics in both intact brain and dissociated NSCs to determine when and how Lgl is restored to the membrane following mitosis. Our results showed that Lgl becomes rapidly restored to the membrane at the completion of mitosis, beginning near the cytokinetic pore connecting the nascent sibling cells (Fig. 1H-J), like what has been observed in follicular epithelial cells[21].

Our results provide a detailed characterization of Lgl's dynamic localization throughout the cell cycle in NSCs, revealing precise spatial and temporal control of its membrane association (Fig. 1K). The patterned removal of Lgl from the membrane during prophase and its rapid restoration post-mitosis suggest the existence of tightly regulated mechanisms controlling Lgl localization.

aPKC removes Lgl from the NSC early in mitosis

Lgl can be removed from the membrane by aPKC but also by the mitotic kinase Aurora A[5,6]. We sought to determine whether one or both kinases are responsible for the patterned removal of Lgl from the membrane during prophase. To dissect the relative contributions of aPKC and Aurora A to Lgl removal, we separately inhibited aPKC or Aurora A activity and assessed the effect on Lgl localization dynamics. We inhibited aPKC by expressing a UAS-controlled aPKC RNAi specifically in larval brain NSCs using Worniu-GAL4 driven expression. For Aurora A inhibition, we added the specific inhibitor MLN8237[6] to the larval brain explant culture media.

In NSCs where aPKC was depleted by RNAi, we observed that Lgl removal from the membrane in mitosis was largely inhibited (Fig. 2A,B; Video 4). Unlike wild type NSCs where we were unable to detect Lgl at the apical membrane late in prophase, aPKC RNAi NSCs had persistent Lgl membrane enrichment throughout mitosis. However, we did detect a small decrease in apical Lgl membrane signal beginning in early prophase indicating that aPKC is not the only kinase that removes Lgl in NSCs, and/or there is residual aPKC activity in aPKC RNAi NSCs. The retention of Lgl on the membrane in aPKC-depleted cells indicates that aPKC-mediated phosphorylation is the key mechanism driving Lgl dissociation from the cell cortex as NSCs enter mitosis. Interestingly, we also observed an increase in Lgl's membrane enrichment during interphase in aPKC RNAi NSCs (Fig. 2A,B), suggesting that Lgl exchanges between the membrane and cytoplasm due to phosphorylation and dephosphorylation in wild type NSCs.

Consistent with our results indicating that aPKC is the dominant kinase responsible for displacement of Lgl from the membrane in NSCs, we found that inhibition of Aurora A activity using MLN8237, did not cause a significant difference in Lgl removal from the membrane compared to wild-type NSCs (Fig. 2C,D; Video 5). The patterned removal of Lgl from the membrane proceeded with similar dynamics and extent as observed in untreated cells. However, we did observe cytokinesis defects in drug treated NSCs (Fig. 2C; Video 5) indicating that Aurora A was successfully inhibited. We conclude that, despite its known ability to phosphorylate Lgl, Aurora A does not participate in removal of Lgl from the NSC

membrane. This conclusion is consistent with a previous study that found the Aurora A phosphorylation sites on Lgl were dispensable for its removal from the membrane in NSCs[5].

aPKC patterns Lgl membrane clearance

Given our findings implicating aPKC as the primary kinase responsible for Lgl removal from the membrane during prophase, we next sought to determine whether the spatial and temporal dynamics of aPKC localization are consistent with the observed pattern of Lgl removal. The recruitment of aPKC to the membrane in early prophase is a complex, multistep process where aPKC is initially localized to small domains on the apical surface before coalescing into an apical cap by metaphase[22,23]. To determine the interplay between Lgl's disappearance and aPKC's appearance on the membrane, we simultaneously imaged aPKC-GFP (expressed from its endogenous promoter) and Lgl-mCherry (expressed by Worniu-GAL4 driven UAS) in NSCs. This approach allowed us to directly correlate the spatial and temporal dynamics of aPKC recruitment with the pattern of Lgl removal from the cell membrane. We observed that Lgl removal at the apical pole of the NSC was tightly correlated with the appearance of aPKC at that site (Fig. 3A,B; Video 6). The correlation between aPKC's appearance and Lgl's disappearance from the membrane continued until aPKC was fully targeted to the apical membrane. However, Lgl's removal from the membrane continued after aPKC targeting was completed. We conclude that aPKC removes Lgl from the membrane both directly, by removing it from membrane regions that it occupies, and indirectly. Indirect removal of basal Lgl by apical aPKC is likely influenced by factors such as the rate of Lgl diffusion along the plasma membrane.

Lgl excludes basal aPKC by regulating aPKC interphase membrane association

The mutual exclusion model, which posits that Lgl and the Par complex reciprocally control each other's localization by occupying an opposing membrane domain, does not explain the behavior of these proteins in NSCs or SOPs. The primary inconsistency is the metaphase polarized state when the Par complex polarized while Lgl is cytoplasmic. However, it is also not known whether Lgl regulates aPKC's cytoplasmic localization in interphase. To gain insight into how Lgl regulates Par complex localization in these contexts, we examined aPKC localization in NSCs expressing Lgl RNAi (Worniu-GAL4 driven UAS). In wild-type NSCs, aPKC is typically excluded from the cell membrane during interphase. However, in Lgl-depleted NSCs, we observed a key difference from wild type NSCs where aPKC rapidly returns to the cytoplasm at the end of mitosis. Rather than rapidly dissipating from the membrane, aPKC remained on the membrane throughout interphase in the absence of Lgl (Figure 4A,B; Video 7).

This observation indicates that Lgl plays a crucial role in regulating the interphase membrane localization of aPKC, preventing its premature association with the cell cortex.

As Lgl RNAi NSCs progressed into mitosis, we observed aPKC at the basal membrane and this signal persisted through metaphase (Fig. 4A,C; Video 7). Importantly, our results suggest that the presence of aPKC on the basal membrane during metaphase in Lgl-depleted NSCs is not due to new recruitment during mitosis. Instead, it appears to result from aPKC that remained associated with the membrane throughout interphase. Despite the aberrant basal localization of aPKC in Lgl-depleted NSCs, we observed that the positive signals responsible for recruiting aPKC to the apical membrane in wild-type NSCs remain in Lgl RNAi cells. We observed an increase in apical aPKC from early prophase to metaphase indicating that Lgl is not required for apical recruitment of the Par complex in NSCs. In fact, even though aPKC is present on the basal membrane, the recruitment to the apical membrane leads to metaphase polarity (Fig. 4A,D; Video 7). Thus, the defects caused by loss of Lgl function aren't strictly due to the loss of Par polarity, but instead are due to the presence of basal Par complex. These results provide important insights into how Lgl regulates Par complex localization in NSCs, revealing a more nuanced picture than that suggested by the mutual exclusion model. Lgl appears to play a critical role in preventing premature membrane association during interphase by ensuring proper removal from the membrane during mitotic exit (Fig. 4E).

Discussion

How Lethal giant larvae (Lgl) controls Par complex polarity is a key outstanding question in animal cell polarity. Evidence from localization studies and mutant phenotypes in epithelial cells support a mutual exclusion model in which Lgl and the Par complex control one another's localization by occupying a reciprocal membrane domain[4,24]. This model suggests that depolarization of the Par complex in the absence of Lgl function could result from defects in asymmetric targeting – rather than being targeted to a polarized membrane domain, the Par complex is targeted uniformly to the membrane. However, this model fails to explain Par polarity in sensory organ precursor cells (SOPs) and neural stem cells (NSCs), where Lgl is cytoplasmic during mitosis while the Par complex remains polarized[5,15]. We aimed to resolve this discrepancy and elucidate the mechanism by which Lgl polarizes the Par complex in NSCs when it isn't present on the membrane during mitosis. Our results support a model distinct from mutual exclusion, where Lgl plays a key role in establishing the starting point for NSC and SOP polarity in which the Par complex is not present on the membrane.

Our results indicate that Lgl is not required for polarized targeting of the Par complex. We observed enrichment at the apical membrane in NSCs lacking Lgl function. This led to a state in which the Par complex is present on the basal membrane, but more concentrated at the apical membrane. Thus, Lgl isn't strictly required for Par polarity, since the Par complex is asymmetric in Lgl RNAi NSCs. Instead, Lgl is critical for ensuring that the Par complex isn't present on the basal membrane when apical targeting of the complex begins in early prophase. Basal Par complex, even at the reduced levels we observed compared to apically-enriched complex, is sufficient to disrupt the polarity of downstream components such as Miranda, which become cytoplasmic in *lgl* mutants[14].

These findings suggest a revised model for Lgl's role in controlling Par complex polarity in NSCs. Rather than acting through mutual exclusion during mitosis, Lgl primarily functions to ensure the complete removal of the Par complex from the membrane at the end of mitosis. This removal is crucial for resetting the cell's polarity state, allowing for proper polarization in the subsequent cell cycle. Our results highlight the importance of considering the entire cell cycle when studying polarity regulation. The effect of Lgl on Par complex localization during interphase has profound consequences for mitotic polarization, even though Lgl itself is cytoplasmic during this phase. This study also underscores the context-dependent nature of polarity regulation. While the mutual exclusion model may accurately describe Lgl-Par complex interactions in epithelial cells, it does not fully capture the dynamics in NSCs.

The mechanism by which Lgl removes aPKC from the membrane at the end of mitosis remains an intriguing question. There are several possibilities based on our current understanding of Lgl and aPKC. One potential mechanism is that Lgl, upon its rapid return to the membrane post-mitosis, could act as a competitive inhibitor for aPKC membrane binding sites. Lgl's strong affinity for the membrane[12,13] might allow it to outcompete aPKC and displace it from the membrane. Alternatively, Lgl could recruit or activate a phosphatase that dephosphorylates aPKC or its binding partners, thereby reducing aPKC's affinity for the membrane. Further investigation into these potential mechanisms will be crucial for fully understanding Lgl's role in polarity regulation.

Resource Availability

Lead Contact

Contact the Lead Contact, Kenneth Prehoda (prehoda@uoregon.edu), for further information or to request resources and reagents.

Materials Availability

No new reagents were generated in this study.

Data and Code Availability

Raw data available from the corresponding author on request.

Experimental Model and Subject Details

Fly Strains

Tissue specific expression of UAS controlled transgenes in NSCs was achived using a Worniu-GAL4 driver line. Lgl dynamics were imaged using UAS-Lgl-GFP and the membrane marker UAS-PLCδ-PH-mCherry, which expresses the pleckstrin homology domain of human PLCδ tagged with mCherry and binds to the plasma membrane lipid phosphoinositide PI(4,5)P_2 as a fiduciary marker. The specific mitotic stages were monitored using the chromosome marker His2A-RFP. aPKC and Lgl co-imaging was achieved using UAS-Lgl-mCherry to monitor Lgl localization. and the BAC-encoded-GFP-aPKC [25] was used to monitor aPKC localization. Worniu-Gal4 was used to express UAS-RNAi against aPKC and Lgl in NSCs. Knockdown was enhanced through the coexpression of UAS-Dicer2.

Method Details

Live Imaging

Third instar larvae were incubated at 30 ºC for at least 48 hours prior to imaging and dissection. The brain lobes and ventral nerve cord were dissected in Schneider's Insect Media (SIM) from each larvae, and mounted on a sterile poly-D-lysine coated 35mm glass bottom dish (ibidi Cat#81156) containing modified minimal hemolymph-like solution (HL3.1). Each brain was imaged using a Nikon Eclipse Ti-2 Yokogawa CSU-W1 SoRa spinning disk microscope with dual Photometrics Prime BSI sCMOS cameras, utilizing a 60x water immersion objective. GFP-tagged proteins were visualized using 488 nm illumination, while RFP and mCherry tags were excited with 561 nm light. Super-resolution images were captured via SoRa (super-resolution through optical photon reassignment) optics, as described by Azuma and Kei (2015). Neuroblasts were distinguished based on size, central nervous system location, and expression of the Worniu-GAL4 neuroblast-specific driver line.

To acquire "dissociated NSCs", *Drosophila* central nervous systems were collected from third instar larvae and incubated for 30 min at 30°C in Schneider's Insect Medium containing 1mg/mL Papain and 1mg/mL Collagenase. After incubation, mechanical dissociation was achieved by flushing medium/brains through a pipette tip. The resulting cell suspension was then pelleted using gentle centrifugation and washed 3 times with culture medium consisting of Schneider's Insect Medium containing 10% synthetic fetal bovine serum, 20mM Glutamine, 0.05mg/mL

Glutathione, and 0.01mg/mL Insulin. After the final wash step, cells were resuspended and plated in the previously described culture medium and imaged.

Pharmacological Inhibition

The selective Aurora A inhibitor MLN8237 (Alisertib) was used at a working concentration of 15µm solubilized in DMSO in all relevant experiments.

Image Processing and Analysis

Imaging data was processed using ImageJ (FIJI package). For some movies, the bleach correction tool was used to correct for photobleaching.

Quantification for Figure 1D To quantify patterned Lgl removal, NSCs were analyzed by identifying the frame where the apical membrane-to-cytoplasm ratio neared 1, indicating complete Lgl removal. A 5-pixel line perpendicular to the apical membrane was used to capture the membrane signal, and a cytoplasmic value was obtained from a square region excluding the nuclear envelope. This ratio was measured at both the apical and lateral regions.

Quantification for Figure 1H: To quantify patterned Lgl removal in dissociated NSCs (n=3), the same method of measuring the membrane to cytoplasmic ratio as was used in figure 1D was used, in which the frame where the apical membrane to cytoplasm ratio neared 1 was identified, and the apical membrane to cytoplasmic ratio and the equatorial membrane to cytoplasmic ratio was measured to show depletion of Lgl.

Quantification for Figure 1G: For basal Lgl removal in dissociated NSCs, the same quantification method as used for the previous figure was applied. The basal membrane-to-cytoplasm ratio was plotted relative to metaphase, which was defined as the frame before anaphase onset. Anaphase onset was defined as the frame where chromosome separation from the metaphase plate first occurred, using His2A-RFP-tagged chromosomes or UAS-Lgl-GFP after nuclear envelope breakdown as a chromosomal marker.

Quantification for Figure 1J: To quantify Lgl reloading, UAS-Lgl-GFP dissociated neural stem cells (NSCs) were used, as these provided a clearer view of the basal side compared to in-tissue cells. In these cells, Lgl appears to be recruited first to the basal cortex. The analysis identified the first frame during anaphase in which Lgl was fully cytoplasmic. Anaphase was defined as any time after the chromosomes had visibly separated. This frame was designated as the "Pre-reloading" time point. The next key frame was where Lgl reloading was observed at both the midbody and lateral cortex, which was labeled as the "Reloading" time point. The final frame of each movie, where Lgl was confirmed to be uniformly cortical, was taken as the "Cortical" time point. At each of these time points, the membrane-to-cytoplasm Lgl ratio was measured using the previously described method at three locations: the midbody, the lateral (equatorial) cortex, and the apical cortex. The lateral cortex was defined as the equator of the cell, and the apical side was positioned opposite the midbody. The membrane-to-cytoplasm ratios at the midbody, lateral, and apical regions were quantified at the pre-reloading, reloading, and cortical time points for each UAS-Lgl-GFP NSC.

Quantification for Figure 2B: To quantify ectopic membrane-bound Lgl in the aPKC RNAi condition, UAS-Lgl-GFP cells were first analyzed to confirm the typical pattern of Lgl localization. Lgl was fully membrane-bound during interphase (15 minutes before nuclear envelope breakdown, NEB), partially removed in early mitosis (7 minutes before NEB), and completely removed by metaphase (defined as one frame before anaphase onset). The membrane-to-cytoplasmic Lgl ratio was measured at these time points for both the control (UAS-Lgl-GFP n =5) and aPKC RNAi (n=5), using the quantification method described in Figure 1.

Quantification for Figure 2D: To quantify the cortical removal of Lgl during aurA inhibition, each movie was analyzed to identify two key time points: (1) the last frame before nuclear envelope breakdown (NEB) where Lgl was fully cortical, and (2) the frame where Lgl was completely cleared in relation to anaphase onset in DMSO control cells. The earliest usable time point was 6 minutes and 40 seconds before NEB. Lgl was fully removed by metaphase, defined as the frame immediately preceding anaphase onset. These time points were designated as "Early Mitosis" and "Metaphase," respectively. The membrane-to-cytoplasmic ratio at the apical region was measured using previously described methods for both time points. Comparisons were made between aurA-inhibited cells (n=3) and DMSO control cells (n=3) for the early mitosis and metaphase time points.

Quantifications for Figure 3B: To quantify the simultaneous release of Lgl and recruitment of aPKC at the apical pole, the frame marking the initial clearance of Lgl from the apical membrane was selected for analysis. In this frame, the apical membrane-to-cytoplasmic ratio was calculated for cells co-expressing BAC aPKC-GFP and UAS-Lgl-mCherry using previously established methods (N=3).

Quantification for Figure 4B: To quantify aPKC-GFP in the apical region in the Lgl-RNAi condition, the same timepoints as the aPKC-RNAi experiment in figure 2 were used. It was first confirmed that at interphase (15 minutes pre NEB) that wildtype aPKC was completely cytoplasmic. It was then confirmed at early mitosis (7 minutes pre NEB) that aPKC was just beginning to localize to the apical membrane. By metaphase, which again was defined as the frame before anaphase onset, wildtype aPKC is strongly localized at the apical crescent. The apical membrane to cytoplasmic ratio was measured for both Lgl-RNAi cells (n=3) and WT-aPKC cells (n=3).

Quantifications for Figure 4C: To quantify ectopic basal aPKC in the Lgl-RNAi condition, it was determined in WT aPKC cells that aPKC was fully polarized on the apical membrane, and completely absent from the basal membrane by metaphase, which was determined to be the frame before anaphase onset.

Statistical Analysis

Gardner-Altman estimation plots and 95% confidence intervals of datasets were prepared using the DABEST package [26]. Statistical details can be found in the relevant methods section and figure legends.

Key Resources Table

REAGENT or RESOURCE	SOURCE	IDENTIFIER
Experimental Model: Fly Strains		
BacaPKC-GFP	François Schweisguth Lab; (Besson et al., 2015)	PMID: 25843034
UAS-Lgl-GFP	Juergen A. Knoblich Lab; (Writz-Peitz et al., 2008)	PMID: 25484300
Endogenous Lgl-GFP	Bloomington *Drosophila* Stock Center (BDSC)	BDSC Cat#63183 RRID: BDSC 63183
His2a-RFP (chromosome marker)	Bloomington *Drosophila* Stock Center (BDSC)	BDSC Cat# 23650 RRID: BDSC 23650
Worniu-GAL4 (NSC driver line)	Chris Q. Doe Lab	
aPKC-RNAi	Bloomington *Drosophila* Stock Center (BDSC)	BDSC Cat#67204 RRID: BDSC 67204
Lgl-RNAi	Bloomington *Drosophila* Stock Center (BDSC)	BDSC Cat#38989 RRID: BDSC 38989
UAS-Lgl-mCherry	Bloomington *Drosophila* Stock Center (BDSC)	BDSC Cat#31776 RRID: BDSC 31776
UAS-PLCδ-PH-mCherry (membrane marker)	Bloomington *Drosophila* Stock Center (BDSC)	BDSC Cat#51658 RRID: BDSC 51658
Pharmacological Inhibitors		
MLN8237 (Alisertib)	Selleckchem	Cat#S1133

Acknowledgments

We thank Adam Fries for maintaining the microscope used in this study. This work was supported by NIH grants R35GM127092 and K99GM147601.

Author Contributions

B.L. and K.E.P. designed the experiments. B.L. performed the experiments. R.R.P. contributed to the String inhibition and String staining experiments. B.L. and K.E.P analyzed the data, prepared the figures, and wrote the manuscript.

Declaration of Interests

The authors have no competing interests to declare.

Figure Legends

Figure 1 Patterned Lgl displacement and reloading during neural stem cell asymmetric division

(A) Mutual exclusion model for Par polarity. In this model, the Par complex (Par-6 and atypical Protein Kinase C or aPKC) forms a mutually exclusive membrane domain with Lethal giant larvae (Lgl) where the presence of one on the membrane excludes the other. This model fails to account for Drosophila neural stem cells (NSCs) and sensory organ precursors where the Par complex is polarized during mitosis and Lgl is cytoplasmic.

(B) Imaging Drosophila larval brain neural stem cells (NSCs). The larval central nervous system (brain lobes and ventral nerve cord) are isolated from L3 stage larvae and the NSCs, identified by their relatively larger size, are either imaged in the intact CNS or the tissue is dissociated and isolated NSCs are imaged.

(C) Removal of Lgl from the plasma membrane in early mitosis in an NSC from the intact central nervous system. Frames from Video 1 are shown with Lgl-GFP (expressed from Worniu-GAL4 driven UAS) and Histone H2A (His2a-RFP) with the NSC marked with asterisk. Time is shown relative to nuclear envelope breakdown.

(D) Patterned removal of Lgl from the plasma membrane in early mitosis. Lgl's membrane enrichment relative to the cytoplasm is shown for 10 different NSCs at the apical and lateral region in early mitosis when Lgl was first cleared from the apical membrane. Gardner-Altman estimation plot shows the paired measurements for each NSC. The 95% confidence interval is shown in the mean difference comparison along with the bootstrap distribution from which it was derived.

(E) Lgl dynamics across the cell cycle and in the full cell volume. Frames from Video 2 are shown with views of both a medial optical section and the full volume of the NSC reconstructed using a maximum intensity projection (MIP) of optical sections across the cell.

(F) Removal of Lgl from the plasma membrane in early mitosis in an NSC dissociated from the central nervous system. Frames from Video 3 are shown as in (C).

(G) Removal of Lgl from the basal membrane. The time when basal Lgl membrane signal was cleared (membrane to cytoplasmic signal was approximately one) relative to metaphase is shown for three dissociated NSCs.

(H) Lgl reloading to the plasma membrane in early interphase in an NSC from the intact central nervous system. Frames from Video 1 are shown as in (C).

(I) Lgl reloading to the plasma membrane in early interphase in an NSC dissociated from the central nervous system. Frames from Video 3 are shown as in (C).

(J) Lgl patterned membrane reloading in early interphase. Lgl membrane enrichment relative to the cytoplasm is shown for telophase, early interphase, and interphase measured at the midbody, along with the lateral and apical membranes.

(K) Schematic of Lgl membrane dynamics in NSCs. Lgl is bound across the NSC membrane in interphase and is removed starting at the apical pole in early mitosis until it is completely removed in prophase. Membrane reloading begins in early interphase starting near the midbody.

Figure 2 aPKC but not Aurora A is required for Lgl removal from the NSC membrane in early mitosis

(A) Lgl dynamics in an NSC from the intact central nervous system expressing aPKC RNAi. Frames from Video 4 are shown with Lgl-GFP and aPKC RNAi (both expressed from Worniu-GAL4 driven UAS). Time is shown relative to nuclear envelope breakdown. The same timepoints are shown from an NSC not expressing aPKC RNAi (”WT”) for comparison.
(B) aPKC is required for Lgl removal from the membrane in early mitosis. The apical Lgl membrane enrichment relative to the cytoplasm is shown for aPKC RNAi or WT NSCs in interphase, prophase, and metaphase.
(C) Lgl dynamics in an NSC from the intact central nervous system incubated with the specific Aurora A inhibitor MLN8237. Frames from Video 5 are shown with Lgl-GFP and aPKC RNAi (both expressed from Worniu-GAL4 driven UAS). Arrowheads highlight furrow retraction in late cytokinesis. Time is shown relative to anaphase onset. Similar timepoints are shown from an NSC incubated with the solvent used for the inhibitor (”DMSO”).
(D) No detectable effect of Aurora A inhibition on Lgl membrane displacement in early mitosis. The apical Lgl membrane enrichment is shown for drug- or solvent-only-treated NSCs prophase and metaphase.

Figure 3 Patterned Lgl removal from the apical and basal NSC membrane by apical aPKC
(A) Lgl and aPKC dynamics in an NSC from the intact central nervous system. Frames from Video 6 are shown with aPKC-GFP (expressed from its native promoter) and Lgl-mCherry (expressed from Worniu-GAL4 driven UAS). Time is shown relative to nuclear envelope breakdown.
(B) aPKC is enriched at the apical membrane when Lgl is first cleared. The apical Lgl and aPKC membrane enrichments relative to the cytoplasm are shown for three different NSC divisions.

Figure 4 Lgl regulates aPKC membrane removal at mitotic exit
(A) aPKC dynamics in an NSC from the intact central nervous system expressing Lgl RNAi. Frames from Video 7 are shown with aPKC-GFP (expressed from its native promoter) from an NSC expressing Lgl RNAi (from Worniu-GAL4 driven UAS). Arrowheads highlight basal aPKC near mitotic entry. Time is shown relative to nuclear envelope breakdown. An NSC not expressing Lgl RNAi (”WT”) is shown at similar time points for comparison.
(B) Lgl is required to remove aPKC from the membrane in interphase. Comparison of apical aPKC membrane enrichment between NSCs expressing and not expressing Lgl RNAi at interphase, prophase, and metaphase.
(C) Lgl is required to remove aPKC from the basal membrane at metaphase. Comparison of basal aPKC membrane enrichment between NSCs expressing and not expressing Lgl RNAi at metaphase. Gardner-Altman estimation plot is shown for three different NSC divisions. The error bars represent one standard deviation (gap is mean); the bar in the mean difference comparison represents bootstrap 95% confidence interval.
(D) Lgl is not required for metaphase aPKC polarity. The ratio of apical to basal membrane aPKC at metaphase is shown for three different NSC divisions. The error bars represent one standard deviation (gap is mean).
(E) Model for Lgl function in NSC asymmetric division. Lgl plays a key role in early interphase by removing the Par complex from the membrane. When mitosis begins Lgl’s clearing of the Par complex ensures that only apically targeted complex is present on the membrane allowing fate determinants to polarize to the basal membrane. Without Lgl, the Par complex persists on the membrane through interphase. During mitosis the Par complex is targeted to the apical membrane as in wild type NSCs, but the presence of Lgl on the membrane before recruitment leads to a polarized state where residual Par complex remains on the basal membrane prevents fate determinants from binding the basal membrane.

Video Legends

Video 1: Lgl dynamics in NSCs

Super-resolution videos of in-tissue NSCs expressing UAS-Lgl-GFP (Lgl) and His2a-RFP (His2a). Time relative to anaphase onset is indicated. 3 medical section videos of dividing in-tissue NSCs are shown.

Video 2: Lgl and membrane dynamics in NSCs

Super-resolution videos of in-tissue NSCs expressing UAS-Lgl-GFP (Lgl) and the membrane marker PH- PLCδ-mCherry (membrane). Time relative to anaphase onset is indicated. 3D max intensity projections and medial sections are shown for 3 dividing NSCs.

Video 3: Lgl dynamics in dissociated NSCs

Super-resolution time-lapse videos of dissociated NSCs expressing UAS-Lgl-GFP (Lgl) and His2a-RFP (His2a). Time relative to anaphase onset is indicated. 3 medial section videos of dividing dissociated NSCs are shown.

Video 4 The effects of aPKC knockdown on Lgl dynamics

Super-resolution videos of in-tissue NSCs expressing UAS-Lgl-GFP (Lgl-GFP) and aPKC RNAi. Time relative to anaphase onset is indicated. Medial sections are shown for 6 dividing NSCs.

Video 5: The effects of Aurora A inhibition on Lgl dynamics

Part 1: Lgl dynamics in NSCs treated with Aurora A inhibitor. Super-resolution videos of in tissue NSCs expressing UAS-Lgl-GFP (Lgl) and His2a-RFP (His2a). Time relative to anaphase onset is indicated. Medial sections are shown for 3 dividing NSCs.

Part 2: Lgl dynamics in NSCs treated with DMSO. Super-resolution videos of in-tissue NSCs expressing UAS-Lgl-GFP (Lgl) and His2a-RFP (His2a). Time relative to anaphase onset is indicated. Medial sections are shown for 3 dividing NSCs.

Video 6: Dual imaging of Lgl and aPKC dynamics in NSCs NSCs expression aPKC-GFP and Lgl-mCherry

Super-resolution videos of in-tissue NSCs expressing aPKC-GFP (aPKC) and Lgl-mCherry (Lgl). Time relative to anaphase onset is indicated. Medial sections are shown for 3 dividing NSCs.

Video 7: The effects of Lgl knockdown on aPKC dynamics

Part 1: aPKC dynamics in NSCs expressing Lgl-RNAi. Super-resolution videos of in-tissue NSCs expressing BacaPKC-GFP (aPKC) and Lgl-RNAi. Time relative to anaphase onset is indicated. Medial sections are shown for 3 dividing NSCs.

Part 2: aPKC dynamics in dividing NSCs (Wild-type control). Super-resolution videos of in-tissue NSCs expressing BacaPKC-GFP (aPKC). Time relative to anaphase onset is indicated. Medial sections are shown for 3 dividing NSCs.

References

1. Lang, C. F. & Munro, E. The PAR proteins: from molecular circuits to dynamic self-stabilizing cell polarity. *Dev. Camb. Engl.* **144**, 3405–3416 (2017).
2. Venkei, Z. G. & Yamashita, Y. M. Emerging mechanisms of asymmetric stem cell division. *J. Cell Biol.* (2018) doi:10.1083/jcb.201807037.
3. Sunchu, B. & Cabernard, C. Principles and mechanisms of asymmetric cell division. *Dev. Camb. Engl.* **147**, dev167650 (2020).
4. Buckley, C. E. & St Johnston, D. Apical-basal polarity and the control of epithelial form and function. *Nat. Rev. Mol. Cell Biol.* **23**, 559–577 (2022).
5. Bell, G. P., Fletcher, G. C., Brain, R. & Thompson, B. J. Aurora kinases phosphorylate Lgl to induce mitotic spindle orientation in Drosophila epithelia. *Curr. Biol. CB* **25**, 61–68 (2015).
6. Carvalho, C. A., Moreira, S., Ventura, G., Sunkel, C. E. & Morais-de-Sá, E. Aurora A triggers Lgl cortical release during symmetric division to control planar spindle orientation. *Curr. Biol. CB* **25**, 53–60 (2015).
7. Grifoni, D. *et al.* aPKCzeta cortical loading is associated with Lgl cytoplasmic release and tumor growth in Drosophila and human epithelia. *Oncogene* **26**, 5960–5965 (2007).
8. Yamanaka, T. *et al.* Lgl mediates apical domain disassembly by suppressing the PAR-3-aPKC-PAR-6 complex to orient apical membrane polarity. *J. Cell Sci.* **119**, 2107–2118 (2006).
9. Holly, R. W., Jones, K. & Prehoda, K. E. A Conserved PDZ-Binding Motif in aPKC Interacts with Par-3 and Mediates Cortical Polarity. *Curr. Biol. CB* **30**, 893-898.e5 (2020).
10. Atwood, S. X., Chabu, C., Penkert, R. R., Doe, C. Q. & Prehoda, K. E. Cdc42 acts downstream of Bazooka to regulate neuroblast polarity through Par-6 aPKC. *J. Cell Sci.* **120**, 3200–3206 (2007).
11. Hutterer, A., Betschinger, J., Petronczki, M. & Knoblich, J. A. Sequential Roles of Cdc42, Par-6, aPKC, and Lgl in the Establishment of Epithelial Polarity during Drosophila Embryogenesis. **6**, 845–854 (2004).

12. Bailey, M. J. & Prehoda, K. E. Establishment of Par-Polarized Cortical Domains via Phosphoregulated Membrane Motifs. *Dev. Cell* **35**, 199–210 (2015).
13. Dong, W. *et al.* A conserved polybasic domain mediates plasma membrane targeting of Lgl and its regulation by hypoxia. *J. Cell Biol.* **211**, 273–286 (2015).
14. Peng, C. Y., Manning, L., Albertson, R. & Doe, C. Q. The tumour-suppressor genes lgl and dlg regulate basal protein targeting in Drosophila neuroblasts. *Nature* **408**, 596–600 (2000).
15. Wirtz-Peitz, F., Nishimura, T. & Knoblich, J. A. Linking cell cycle to asymmetric division: Aurora-A phosphorylates the Par complex to regulate Numb localization. *Cell* **135**, 161–173 (2008).
16. Prehoda, K. E. Polarization of Drosophila neuroblasts during asymmetric division. *Cold Spring Harb. Perspect. Biol.* **1**, a001388 (2009).
17. Knoblich, J. A. Asymmetric cell division: recent developments and their implications for tumour biology. *Nat. Rev. Mol. Cell Biol.* **11**, 849–860 (2010).
18. LaFoya, B. & Prehoda, K. E. Actin-dependent membrane polarization reveals the mechanical nature of the neuroblast polarity cycle. *Cell Rep.* **35**, 109146 (2021).
19. LaFoya, B. & Prehoda, K. E. Consumption of a polarized membrane reservoir drives asymmetric membrane expansion during the unequal divisions of neural stem cells. *Dev. Cell* S1534-5807(23)00159–4 (2023) doi:10.1016/j.devcel.2023.04.006.
20. Penkert, R. R. *et al.* The Drosophila neuroblast polarity cycle at a glance. *J. Cell Sci.* **137**, jcs261789 (2024).
21. Moreira, S. *et al.* PP1-Mediated Dephosphorylation of Lgl Controls Apical-basal Polarity. *Cell Rep.* **26**, 293-301.e7 (2019).
22. Oon, C. H. & Prehoda, K. E. Asymmetric recruitment and actin-dependent cortical flows drive the neuroblast polarity cycle. *eLife* **8**, (2019).
23. Oon, C. H. & Prehoda, K. E. Phases of cortical actomyosin dynamics coupled to the neuroblast polarity cycle. *eLife* **10**, e66574 (2021).
24. Lee, C.-Y., Robinson, K. J. & Doe, C. Q. Lgl, Pins and aPKC regulate neuroblast self-renewal versus differentiation. *Nature* **439**, 594–598 (2006).

25. Besson, C. *et al.* Planar Cell Polarity Breaks the Symmetry of PAR Protein Distribution prior to Mitosis in Drosophila Sensory Organ Precursor Cells. *Curr. Biol. CB* **25**, 1104–1110 (2015).

26. Ho, J., Tumkaya, T., Aryal, S., Choi, H. & Claridge-Chang, A. Moving beyond P values: data analysis with estimation graphics. *Nat. Methods* **16**, 565–566 (2019).

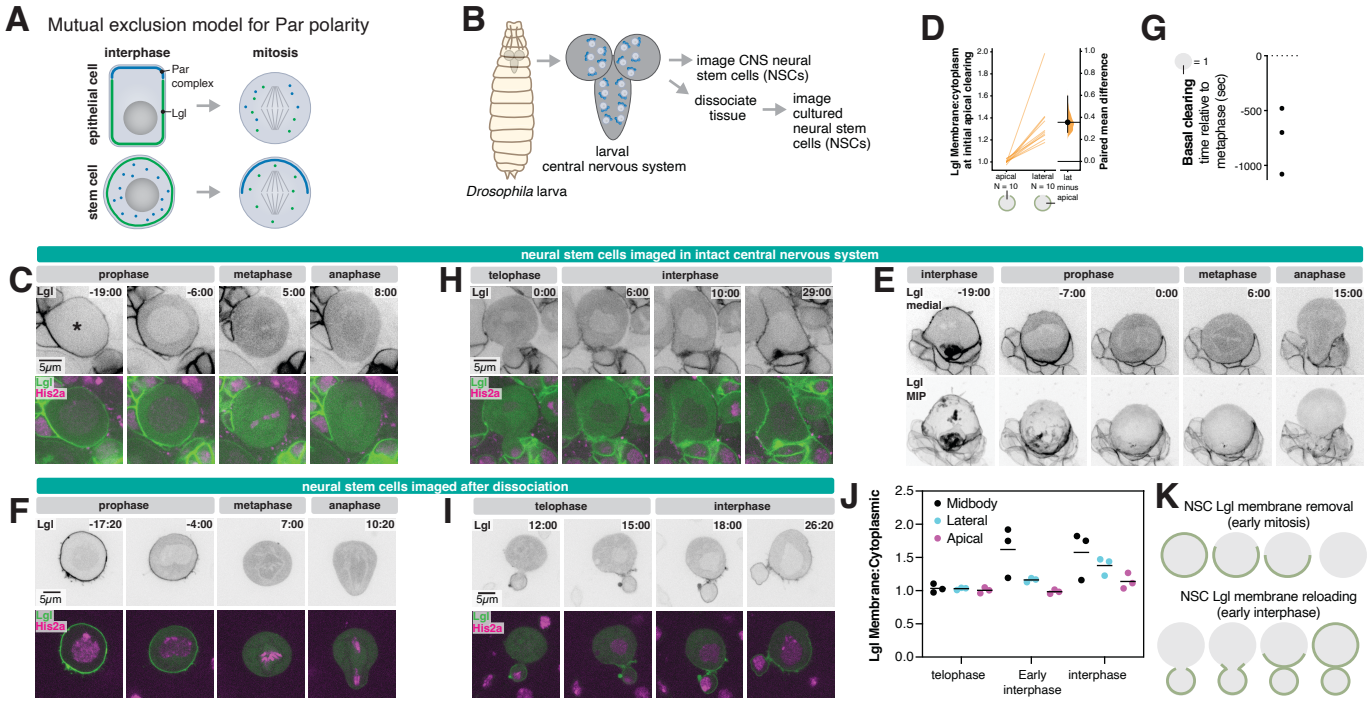
A
Mutual exclusion model for Par polarity
interphase
mitosis
epithelial cell
stem cell
Par complex
Lgl
B
image CNS neural stem cells (NSCs)
dissociate tissue
image cultured neural stem cells (NSCs)
larval central nervous system
Drosophila larva
D
Lgl Membrane:cytoplasm at initial apical clearing
Paired mean difference
apical N = 10
lateral N = 10
lat minus apical
G
Basal clearing
time relative to metaphase (sec)
= 1
0
-500
-1000
neural stem cells imaged in intact central nervous system
C
prophase
metaphase
anaphase
Lgl
-19:00
-6:00
5:00
8:00
5μm
Lgl
His2a
H
telophase
interphase
0:00
6:00
10:00
29:00
E
interphase
prophase
metaphase
anaphase
Lgl medial
-19:00
-7:00
0:00
6:00
15:00
Lgl MIP
neural stem cells imaged after dissociation
F
prophase
metaphase
anaphase
-17:20
-4:00
7:00
10:20
I
telophase
interphase
12:00
15:00
18:00
26:20
J
Midbody
Lateral
Apical
Lgl Membrane:Cytoplasmic
telophase
Early interphase
interphase
K
NSC Lgl membrane removal (early mitosis)
NSC Lgl membrane reloading (early interphase)

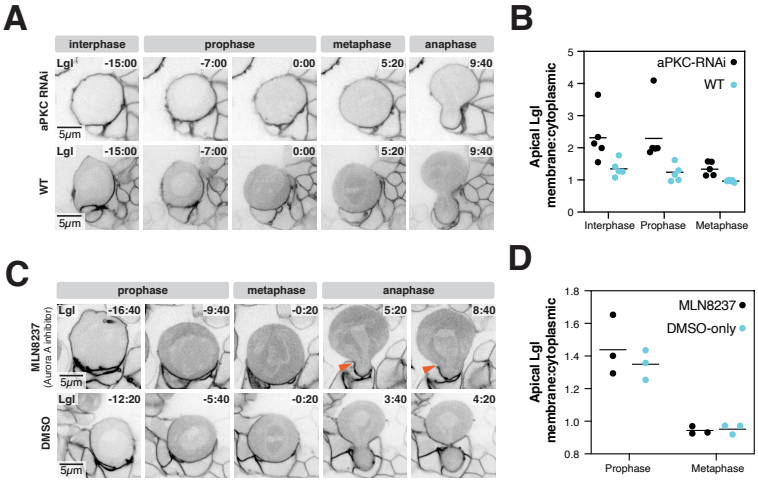
A
interphase
prophase
metaphase
anaphase
aPKC RNAi
WT
Lgl
-15:00
-7:00
0:00
5:20
9:40
5μm
B
aPKC-RNAi
WT
Apical Lgl membrane:cytoplasmic
Interphase
Prophase
Metaphase
C
MLN8237 (Aurora A inhibitor)
DMSO
-16:40
-9:40
-0:20
5:20
8:40
-12:20
-5:40
-0:20
3:40
4:20
D
MLN8237
DMSO-only
Prophase
Metaphase

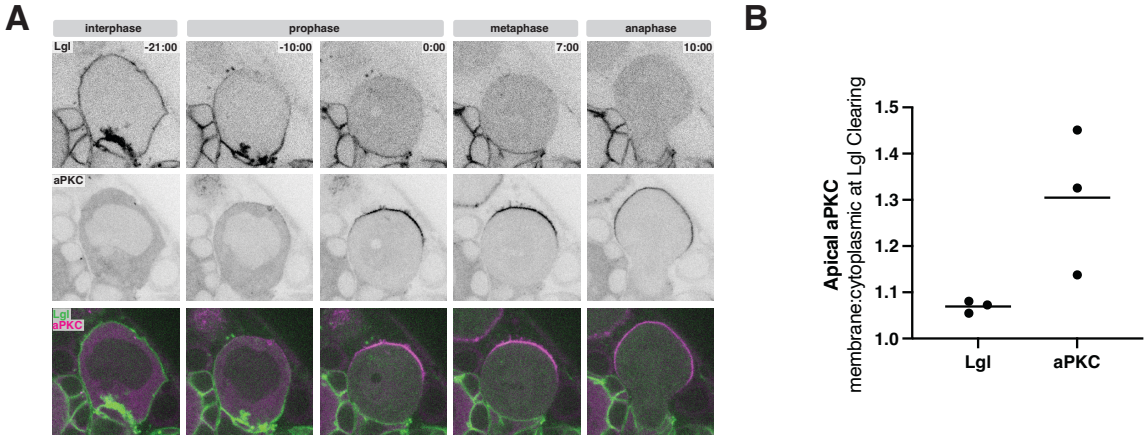
A
interphase
prophase
metaphase
anaphase
Lgl
-21:00
-10:00
0:00
7:00
10:00
aPKC
Lgl
aPKC
B
Apical aPKC
membrane:cytoplasmic at Lgl Clearing
1.5
1.4
1.3
1.2
1.1
1.0
Lgl
aPKC

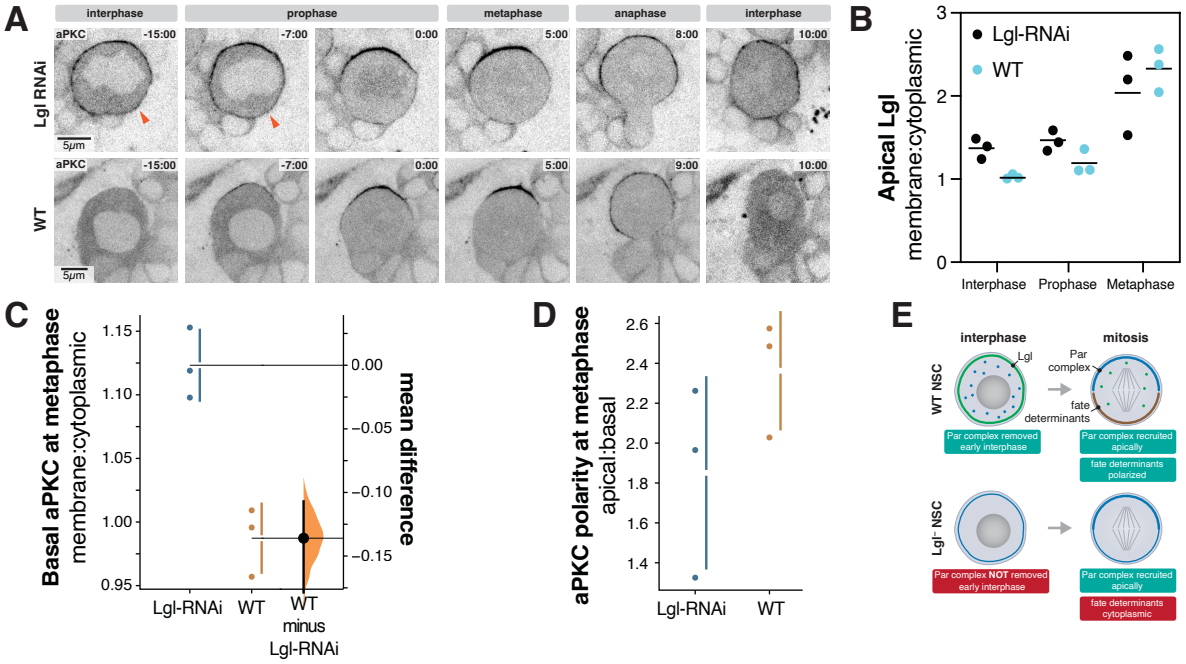
A
interphase
prophase
metaphase
anaphase
interphase
Lgl RNAi
WT
aPKC
-15:00
-7:00
0:00
5:00
8:00
9:00
10:00
5μm
B
Lgl-RNAi
WT
Apical Lgl
membrane:cytoplasmic
Interphase
Prophase
Metaphase
C
Basal aPKC at metaphase
membrane:cytoplasmic
mean difference
Lgl-RNAi
WT
WT minus Lgl-RNAi
D
aPKC polarity at metaphase
apical:basal
Lgl-RNAi
WT
E
interphase
mitosis
WT NSC
Lgl
Par complex
fate determinants
Par complex removed early interphase
Par complex recruited apically
fate determinants polarized
Lgl⁻ NSC
Par complex NOT removed early interphase
Par complex recruited apically
fate determinants cytoplasmic